

Highlights

Nonlinear scintillation effects in the intrinsic luminescence from $\text{Sc}_{1.318}\text{Y}_{0.655}\text{Si}_{1.013}\text{O}_{4.987}$ crystal excited by electrons and γ -quanta

M. V. Belov, V. A. Kozlov, N. V. Pestovskii, S. Yu. Savinov, V. S. Tskhay, V. I. Vlasov, A. I. Zagumennyi, Yu. D. Zavartsev, M. V. Zavertyaev

- Bright intrinsic luminescence from a congruent $(\text{Y}_2\text{Sc}_1)_{0,(3)}(\text{Sc})[\text{Si}]\text{O}_5$ compound is found
- Nonlinear effects in both cathodoluminescence and radioluminescence are analyzed
- A shift in the emission spectrum and a change in the decay time are observed
- The excitation densities are estimated and their effect on scintillation is discussed

Nonlinear scintillation effects in the intrinsic luminescence from $\text{Sc}_{1.318}\text{Y}_{0.655}\text{Si}_{1.013}\text{O}_{4.987}$ crystal excited by electrons and γ -quanta

M. V. Belov^a, V. A. Kozlov^a, N. V. Pestovskii^{a,*}, S. Yu. Savinov^a, V. S. Tskhay^a, V. I. Vlasov^b, A. I. Zagumennyi^b, Yu. D. Zavartsev^b and M. V. Zavertyaev^a

^aP.N. Lebedev Physical Institute of the Russian Academy of Sciences, Leninskii prospekt 53, 119991, Moscow, Russia

^bA.M. Prokhorov General Physics Institute of the Russian Academy of Sciences, Vavilova str. 38, 119991, Moscow, Russia

ARTICLE INFO

Keywords:

scintillation nonlinearity
scandium oxyorthosilicate
yttrium oxyorthosilicate
intrinsic luminescence
density of electronic excitation

ABSTRACT

The spectral and kinetic properties of intrinsic luminescence from $(\text{Y}_2\text{Sc}_1)_{0,(3)}(\text{Sc})[\text{Si}]\text{O}_5$ crystal are studied. The emission is excited by electrons and γ -quanta. The composition $(\text{Y}_2\text{Sc}_1)_{0,(3)}(\text{Sc})[\text{Si}]\text{O}_5$ is the congruent one for Sc_2SiO_5 - Y_2SiO_5 solid solutions. It is found, that the crystal emits fairly bright intrinsic cathodoluminescence (CL) and radioluminescence (RL) at room temperature. In particular, the light yield of scintillation excited by γ -quanta with the energies of 661.7 keV is of 12000 photons/MeV. An increase in the beam flux by ~ 20 times leads to the shift in the maximum CL energy spectral density from 315 to 340 nm and to the decrease in the CL decay time at 415 nm from 1377 ± 3 ns to 1165 ± 1 ns. Simultaneously, the decay time of RL excited by a photoelectron with the energy of 644.7 keV is of 1310 ± 10 ns while a Compton electron with the energy of 477 keV excites RL with the decay time of 1050 ± 10 ns. Also, we observed differences in the CL yield dependencies on the volume-averaged density of electronic excitations (EEs) at different wavelengths. An explanation of the results is given considering the nonlinear scintillation phenomena induced by an interaction between EEs. It is based on a conception that an increase in EE volume density leads to an increase in EEs nonradiative quenching due to these interactions.

1. Introduction

Ionizing radiation produces in a matter the ionization tracks – spatial areas where the most of short-lived electronic excitations (EEs) are concentrated. Most of them are non-equilibrium electrons and holes. A radiative decay of these states leads to scintillation – luminescence from media excited by ionizing radiation. Due to a separation of electrons and holes and their subsequent recombination, scintillation is inherently nonlinear process [1]. Indeed, in general, the scintillation energy of a unit volume of a substance depends nonlinearly on the energy of an ionization radiation absorbed by this volume. Currently, the most studied nonlinear scintillation phenomenon is the nonproportionality of scintillation detectors during the registration of γ -radiation [1, 2, 3, 4, 5, 6, 7, 8, 9, 10, 11]. In this case, the light yield LY of a scintillator is different for different energies of exciting single γ -quanta ($LY = E_{lum}/E_{abs}$, where E_{lum} – energy of emitted luminescence, E_{abs} – energy of absorbed ionizing radiation).

This phenomenon is explained by a dependence of luminescence parameters (intensity, decay time, etc) on the EEs volume density n [1, 2, 3, 4, 5, 6, 7, 8]. An increase in n leads to the increase in the probability of EEs nonradiative quench due to interactions between EEs. This leads to a significant reduction in LY at high n ($\sim 10^{19}$ cm⁻³ and

higher) [9]. Simultaneously, values of n in tracks produced by γ -quanta with different energies are different. Thereby, a combined effect of the two factors – a $LY(n)$ dependence and a dependence of both n values and its spatial distributions in tracks on the energy of an ionizing particle leads to the fact that LY is changed for γ -quanta having different energies.

Another important class of nonlinear scintillation phenomena is associated with a dependence of the luminescence kinetic parameters on n [12, 13, 14, 15, 16, 17, 18, 19, 20, 21, 22]. In particular, it is found [12] that an excitation of luminescence by a synchrotron radiation with quanta energies 3-62 keV have a following feature. If a photon flux is higher than 10^{16} ph. \times s⁻¹ \times cm⁻², the scintillation decay times of many oxide, fluoride and alkali-halide scintillators are significantly decreased in comparison to an excitation with low photon fluxes. Similar phenomena are observed in luminescence from YAG:Ce [13], BaF₂ [13, 14], CdWO₄ [14] and CaWO₄ [15] excited by x-ray radiation of a free electron laser. Also, it is found in Ref. [16] that the decay time of CsI:Tl scintillation excited by γ -quanta with the energy of 6 keV is shorter than the luminescence decay time excited by 661.7 keV γ -quanta.

The luminescence decay time shortening of self-trapped excitons (STE) in CdWO₄ induced by an increase in the exciting laser radiation intensity is studied in Refs. [17, 18]. Similar phenomenon is observed in STE luminescence from CsI [19]. The obtained results were described quantitatively using the conception of an increase in the non-radiative quenching of excitons due to their dipole-dipole interaction with increasing n [17, 18, 19]. A theoretical description of the changes in the CsI:Tl scintillation kinetics excited by γ -quanta with different energies is given in Ref. [20]. A

*Corresponding author

✉ belovmv@lebedev.ru (M. V. Belov); kozlov@lebedev.ru (

V. A. Kozlov); pestovskii@lebedev.ru (N. V. Pestovskii);

pestovsky@phystech.edu (N. V. Pestovskii); savinov@lebedev.ru (

S. Yu. Savinov); vtskhay@lebedev.ru (V. S. Tskhay); vlasov@lsk.gpi.ru (

V. I. Vlasov); zagumen@lsk.gpi.ru (A. I. Zagumennyi); zavart@lsk.gpi.ru (

Yu. D. Zavartsev); zavert@lebedev.ru (M. V. Zavertyaev)

ORCID(s):

proposed model takes into account hot and thermalized EEs diffusion, effect of electric field on EEs evolution, EE trapping, their nonlinear quenching and radiative recombination.

In general, it should be noted that only a few nonlinear scintillation phenomena are currently well understood. In particular, mechanisms of nonlinear scintillation phenomena and their effect on the spectral and kinetic characteristics of scintillation are studied insufficiently. Thereby, their studies represent an important challenge for fundamental research. Simultaneously, studies of nonlinear scintillation phenomena generate significant interest for practical applications because, on the one hand, they deteriorate parameters of scintillation detectors (amplitude resolution, proportionality, LY , etc [4, 23]) and thereby they should be suppressed. On the other hand, a dependence of kinetic parameters on n can be used to create detectors distinguishing a type of registered radiation [21]. Indeed, particles of different types, for example, electrons and α -particles with equal initial energies creates in a matter the ionization tracks with different spatial distribution of n .

Thereby, development of new scintillation materials with a high LY and considerable scintillation nonlinearity generates an interest for practical applications. In this regard, rare-earth oxyorthosilicates with chemical formula Re_2SiO_5 (Re – trivalent rare-earth ion) are promising materials because they have a high chemical and radiative stability, a high mechanical strength, a bright luminescence and a fairly high mass density. Therefore, they are now widely used as high-performance scintillators ($\text{Lu}_2\text{SiO}_5:\text{Ce}$ and its modifications [24, 25, 26, 27], $\text{Gd}_2\text{SiO}_5:\text{Ce}$ [28, 29, 30], etc), active laser media [31], quantum memory devices [32], etc. In this work, the spectral and kinetic properties of luminescence from new oxyorthosilicate $\text{Sc}_{1.318}\text{Y}_{0.655}\text{Si}_{1.013}\text{O}_{4.987}$ crystal [33] excited by high-energy particles - γ -quanta with the energy 661.7 keV and electrons with the energies of 50-300 keV. The nonlinear scintillation properties of this material are observed and discussed.

2. Experimental details

2.1. $\text{Sc}_{1.318}\text{Y}_{0.655}\text{Si}_{1.013}\text{O}_{4.987}$ crystal

A crystal with the chemical formula $\text{Sc}_{1.318}\text{Y}_{0.655}\text{Si}_{1.013}\text{O}_{4.987}$ and the crystal-chemistry formula $(\text{Y}_2\text{Sc}_1)_{0.(3)}(\text{Sc})[\text{Si}]\text{O}_5$ is a new chemical compound belonging to class of oxyorthosilicates developed as a quantum memory storage device [33, 34]. This compound is the congruent one for Sc_2SiO_5 - Y_2SiO_5 solid solutions because it corresponds to the minimal melting temperature for $\text{Sc}_{2-x}\text{Y}_x\text{SiO}_5$ ($0 \leq x \leq 2$) compounds. Indeed, the $(\text{Y}_2\text{Sc}_1)_{0.(3)}(\text{Sc})[\text{Si}]\text{O}_5$ melting temperature is of 2100 K whereas the melting temperature of Sc_2SiO_5 is of 2160 K, and Y_2SiO_5 melting temperature – 2200 K. The mass density ρ_M of $(\text{Y}_2\text{Sc}_1)_{0.(3)}(\text{Sc})[\text{Si}]\text{O}_5$ crystal is of 3.859 g/cm³. Details of $(\text{Y}_2\text{Sc}_1)_{0.(3)}(\text{Sc})[\text{Si}]\text{O}_5$ crystalline structure are published in Ref. [34]. The crystal belongs to the $C2/c$ space group. Sc and Y cations are distributed over the two independent crystallographic positions with the coordination numbers (CN) of 6 and 7,

correspondingly. All Y^{3+} ions are situated in the similar crystallographic positions and occupy 2/3 positions having CN=7. Simultaneously, Sc^{3+} ions occupy all positions with CN=6 and 1/3 positions with CN = 7. The crystal $(\text{Y}_2\text{Sc}_1)_{0.(3)}(\text{Sc})[\text{Si}]\text{O}_5$ was grown using the Czochralski method from an iridium crucible in the 99%Ar + 1%O₂ atmosphere from Sc_2O_3 , Y_2O_3 and SiO_2 initial materials with the mass fractions of the primary substances at least 99.99 wt.%. The crystal was cut into cuboids with the dimensions of $3 \times 3 \times 4$ mm³. Luminescence of these cuboids is studied in this work. Actual chemical composition of studied samples was measured using the technique described in Ref. [34]. Averaging of the compositions measured in different spatial points of the samples shows that the crystals have the following chemical formula: $\text{Sc}_{1.318 \pm 0.011}\text{Y}_{0.655 \pm 0.005}\text{Si}_{1.013 \pm 0.003}\text{O}_{4.987 \pm 0.003}$.

2.2. Luminescence measurements

All studies of $(\text{Y}_2\text{Sc}_1)_{0.(3)}(\text{Sc})[\text{Si}]\text{O}_5$ crystal luminescence characteristics in this work were carried out in air at atmospheric pressure and room temperature.

2.2.1. CL measurements

An effective method of studies the scintillation processes at a high EE density including nonlinear scintillation effects is an analysis of cathodoluminescence (CL) from a substance excited by a high-power pulsed electron beam [35, 36, 37, 38, 39, 40, 41, 42, 43, 44, 45]. A setup for CL excitation and a scheme of measuring the electron beam parameters by an x-ray sensor in this work are similar to that used in Ref. [41]. A CL excitation was carried out by a pulsed electron beam generated by a RADAN-EKSPERT electron accelerator equipped with an IMA3-150E vacuum accelerating diode [37, 46, 47]. A kinetic energies of electrons were of 50-300 keV. Every voltage pulse applied to the accelerating diode led to generation of an electron pulse with the number of 10^{10} - 10^{12} electrons during the explosive electron emission (EEE) [48]. The cross-sectional area of the beam was of 2 cm². Each electron pulse was composed of two components – the “fast” one and the “slow” one. The “fast” component with the duration of ~50 ns was consisted of seven to eight electron bunches with a ~1 ns duration and the time between the nearest bunches was of ~5 ns [41, 42, 49]. After that, the “slow” stage dominated with the duration of ~1 μ s. The beam current in the “slow” stage was of ~ 10^3 times fewer than in the “fast” stage [41, 42]. A repetition rate of the accelerator was of 1 Hz.

A temporal dependence $I_{CL}(t)$ of the CL intensity (kinetics) at different wavelengths was measured using the setup described in Refs. [41, 49]. CL was directed using a 15 m quartz optical fiber into the input slit of a Solar TII MS2004 monochromator with a 1200 gr/mm diffraction grating. Behind the output slit of the monochromator, a Hamamatsu H3695-10 photomultiplier tube (PMT) was mounted. A photocurrent was measured by a Tektronix MSO6-2500 oscilloscope with a bandwidth of 2.5 GHz. A total temporal resolution of the system was of ~1 ns. The long optical fiber was used in order to suppress a high-power

Table 1

 Kinetic parameters of intrinsic CL from $(\text{Y}_2\text{Sc}_1)_{0.(\text{Sc})}(\text{Sc})[\text{Si}]\text{O}_5$ at room temperature (CL excited by an electron beam without passing through a copper foil)

Wavelength, nm	Parameters of fitting by Eq. (1) in the region of 0-50 μs				Parameter of fitting by Eq. (2) in the region of 0-3 μs
	a_1	a_2	τ_1, ns	τ_2, ns	τ, ns
260	-	-	1050 \pm 20	1490 \pm 20	1099 \pm 6
270	0.56	0.44	1023 \pm 6	1522 \pm 8	1081 \pm 3
280	0.57	0.43	1031 \pm 2	1520 \pm 5	1090 \pm 2
290	0.57	0.43	1045 \pm 1	1539 \pm 3	1101 \pm 1
295	0.50	0.50	1027.3 \pm 0.9	1469 \pm 2	1084 \pm 2
300	0.56	0.44	1054.9 \pm 0.8	1536 \pm 2	1108 \pm 1
305	0.52	0.48	1057.8 \pm 0.8	1497 \pm 2	1108 \pm 1
310	0.56	0.44	1066.0 \pm 0.8	1596 \pm 2	1130 \pm 1
320	0.58	0.42	1087.0 \pm 0.7	1657 \pm 2	1155 \pm 1
330	0.59	0.41	1098.4 \pm 0.7	1727 \pm 3	1175 \pm 1
335	0.61	0.39	1096.2 \pm 0.7	1813 \pm 3	1187 \pm 1
340	0.60	0.40	1106.9 \pm 0.7	1788 \pm 3	1193 \pm 1
345	0.58	0.42	1105.5 \pm 0.7	1752 \pm 2	1190 \pm 1
350	0.58	0.42	1126.5 \pm 0.7	1790 \pm 2	1211 \pm 1
360	0.59	0.41	1121.4 \pm 0.7	1868 \pm 3	1222 \pm 1
365	0.56	0.44	1109.6 \pm 0.7	1870 \pm 3	1223 \pm 1
370	0.53	0.47	1157.2 \pm 0.7	1817 \pm 2	1248 \pm 1
380	0.55	0.45	1130.5 \pm 0.7	1910 \pm 2	1249 \pm 1
385	0.58	0.42	1106.7 \pm 0.7	2019 \pm 3	1250 \pm 1
390	0.58	0.42	1094.2 \pm 0.7	2088 \pm 4	1254 \pm 1
400	0.62	0.38	1085.1 \pm 0.6	2334 \pm 6	1278 \pm 1
410	0.60	0.40	1065.5 \pm 0.7	2403 \pm 7	1293 \pm 1
420	0.54	0.46	997.2 \pm 0.7	2380 \pm 7	1279 \pm 2
430	0.61	0.39	1063.0 \pm 0.6	2695 \pm 10	1335 \pm 2
440	0.61	0.39	1055.0 \pm 0.6	2810 \pm 11	1350 \pm 2
450	0.63	0.37	1046.1 \pm 0.5	3075 \pm 11	1371 \pm 2

electromagnetic noise generated by the high-current electron accelerator. A transmission region of the fiber was of 250-1000 nm.

The energy spectral density of CL (spectrum) was measured similar to Refs. [41, 49] using an OCEAN FLAME-S-XR1-ES spectrometer in the region of 200-1000 nm. CL was directed into the entrance slit of this spectrometer by a 1 m quartz optical fiber. In this case, we used a short fiber because this spectrometer is based on a semiconductor photodetector. Thereby, it is less sensitive to the accelerator electromagnetic noise than the PMT. An exposure time during the CL spectra measurements was of 5 s for a beam without its passage through a copper foil and 65 s in the case of a passage of an exciting electron beam through a filter based on a copper foil (see the end of this section).

Along with the CL spectrum and kinetics, during the CL measurements, an energy of an exciting electron beam was also determined. Using this value, we then obtained the volume-averaged value of n in a studied crystal. A method of electron beam energy measurement and a method of volume-averaged EE density determination is completely described in Ref. [41]. In this work, similar methods and setup were used. An energy of exciting electron beam was measured by an analysis of x-ray radiation induced by the exciting

electron beam. This x-ray radiation was measured using an x-ray sensor based on a plastic polystyrene: POPOP+ π -terphenyl scintillator. This scintillator was covered with a 20 mkm aluminum foil and was mounted at a distance of 3 cm from the beam axis. The aluminum foil was used as a filter passing the x-ray radiation with the energy quanta higher than 4 keV.

Thereby, the sensor registered the hard component of x-ray radiation. The luminescence from the sensor was transported through the separate channel of the 15 m fiber into the entrance window of a FEU-85 PMT. Its photocurrent was measured by the same Tektronix MSO6-2500 synchronously with the CL signal. Let us denote a temporal dependence of the x-ray intensity as $I_{REF}(t)$. The x-ray energy E_{REF} is proportional to the integral of $I_{REF}(t)$ over time - $E_{REF} \propto \int_0^{\tau_b} I_{REF}(t)dt$, where $\tau_b = 1000$ ns – the time of electron beam existence. Previously [41] we shown that E_{REF} in the conditions of our experiment is directly proportional to energy of exciting electron beam.

Along with the CL characteristics of the crystal studied by an electron beam generated by the vacuum diode, we also studied the CL characteristics from a crystal excited by an electron beam after the passing through a barrier filter made of a copper foil with the thickness of 40 μm . This filter

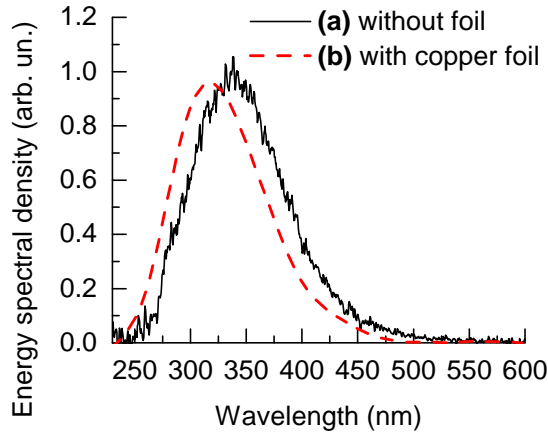


Figure 1: (a) CL spectrum of $(\text{Y}_2\text{Sc}_1)_{0.(3)}(\text{Sc})[\text{Si}]\text{O}_5$ crystal (excitation by an original beam). (b) CL spectrum of the same crystal excited by a beam passed through a $40\ \mu\text{m}$ copper foil.

insignificantly transforms the beam electron energy distribution function (EEDF). However, this filter significantly (~ 1 order of magnitude) reduces the flux of the exciting electron beam and thereby reduces \bar{n} (volume-averaged density of EEs) created by the beam.

2.2.2. RL measurements

Radioluminescence (RL) from a $(\text{Y}_2\text{Sc}_1)_{0.(3)}(\text{Sc})[\text{Si}]\text{O}_5$ crystal was excited by the monochromatic γ -radiation with the photon energy of 661.7 keV emitted by a ^{137}Cs radioactive source. In this work, we measured an empirical distribution function (EDF) of the RL energies (further in this work – amplitude spectrum). Measurements of the amplitude spectrum were made using a classical scheme. A sample was mounted directly to the PMT Hamamatsu R4125Q input window via an optical coupling with an optical grease. Separate RL pulses arisen with a frequency of 10-1000 Hz. The emission was detected by the PMT. A corresponding photocurrent was amplified by a Canberra 2007B preamp, then by a spectrometric amplifier Polon 1101. A signal from this device was registered by an Analog-to-digital converter ADC Schlumberger JCAN-21C. A statistical analysis and formation of EDF was made using a personal computer. A duration of a data accumulation was of ~ 1 hour. As a result, a distribution of the number of scintillations per RL energy E_{RL} was obtained where $E_{RL} \propto \int I_{RL}(t)dt$ (here $I_{RL}(t)$ is a temporal dependence of the RL intensity). In order to study the RL kinetics, a similar scheme with the same PMT Hamamatsu R4125Q and an optically-coupled crystal was used. However, a signal from the PMT was measured in this case similarly to Sec.2.2.1 by a Tektronix MSO6-2500 BW oscilloscope with a bandwidth of 2.5 GHz. Using this setup, $\sim 10^4$ separate $I_{RL}(t)$ was measured and analyzed.

3. Results and discussion

3.1. CL spectra of $\text{Sc}_{1.318}\text{Y}_{0.655}\text{Si}_{1.013}\text{O}_{4.987}$ crystal

The CL spectrum of $(\text{Y}_2\text{Sc}_1)_{0.(3)}(\text{Sc})[\text{Si}]\text{O}_5$ crystal is presented in Fig. 1. It is seen that at room temperature $(\text{Y}_2\text{Sc}_1)_{0.(3)}(\text{Sc})[\text{Si}]\text{O}_5$ crystal emits a fairly bright intrinsic luminescence. The maximal energy spectral density of CL excited by the electron beam without passage through a barrier filter is at 340 nm. In general, the CL spectrum of $(\text{Y}_2\text{Sc}_1)_{0.(3)}(\text{Sc})[\text{Si}]\text{O}_5$ is analogous to the spectra of intrinsic luminescence from oxides containing Sc^{3+} ions in their structures - LuScSiO_5 [50], Sc_2SiO_5 [51, 52] and Sc_2O_3 [53, 54]. However, the wavelengths of the maximal luminescence energy spectral density slightly differ for these materials.

We obtained the following important result. If the fluence of the exciting electron beam is weakened by its passage through a copper foil with the thickness of $40\ \mu\text{m}$, the maximum of CL spectra is shifted to 315 nm (Fig. 1b). Our Monte-Carlo calculations using GEANT4 code shown that a passing of the electron beam through the $40\ \mu\text{m}$ leads to the decrease in the flux of the passed beam by ~ 20 times in comparison to the incident beam. Simultaneously, the foil leads to an insufficient little change in the EEDF of the beam which can be neglected in our analysis. A decrease in the beam flux leads to the decrease in the average EE density produced by the beam (detailed discussion in Sec. 3.5.). Thereby, Fig. 1 shows that a decrease in the EE density leads to the shift of the maximum in $(\text{Y}_2\text{Sc}_1)_{0.(3)}(\text{Sc})[\text{Si}]\text{O}_5$ CL spectrum to shorter wavelengths.

3.2. CL kinetics of $\text{Sc}_{1.318}\text{Y}_{0.655}\text{Si}_{1.013}\text{O}_{4.987}$ crystal

The kinetics of CL from $(\text{Y}_2\text{Sc}_1)_{0.(3)}(\text{Sc})[\text{Si}]\text{O}_5$ crystal at 300, 340 and 440 nm excited by an electron beam without passage through a filter are presented in Fig. 2. The CL kinetics of $(\text{Y}_2\text{Sc}_1)_{0.(3)}(\text{Sc})[\text{Si}]\text{O}_5$ in all our experiments are composed of two stages. At the initial stage, the decay is single-exponential with the decay time of $\sim 1\ \mu\text{s}$. Then the decay transforms into the hyperbolic stage. All observed curves are described fairly accurately by a following expression:

$$I(t) = a_1 \exp\left(-\frac{t}{\tau_1}\right) + \frac{a_2}{\left(1 + \frac{t}{\tau_2}\right)^2}, \quad (1)$$

where a_1 , τ_1 , a_2 and τ_2 are the fitting parameters. In Fig. 2, the results of fitting for $I_{CL}(t)$ at 300, 340 and 440 nm by Eq. (1) are presented. The exponential decay occurs at 0-3 μs . The hyperbolic decay dominates from $\sim 10\ \mu\text{s}$ and corresponds to the Becquerel law with the power -2. This type of a radiative decay occurs due to a two-particle recombination of electrons and holes and thereby this process is a nonlinear scintillation phenomenon [1].

The fitting parameters of $I_{CL}(t)$ by Eq. (1) are presented in Table 1. The parameters a_1 and a_2 at all wavelengths are normalized on their sum $a_1 + a_2$. This corresponds to

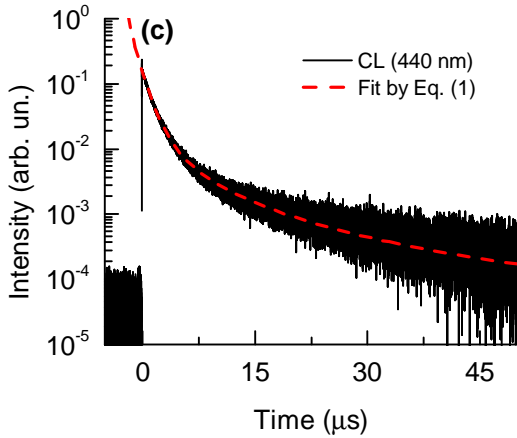
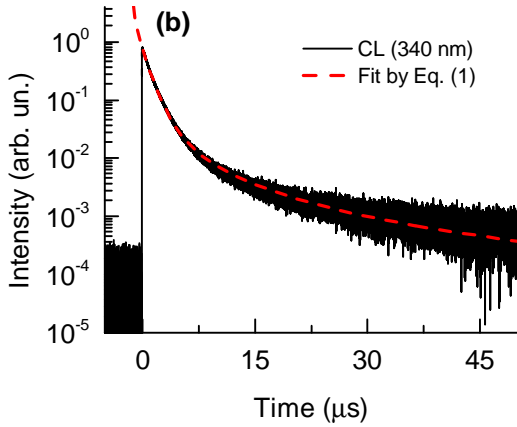
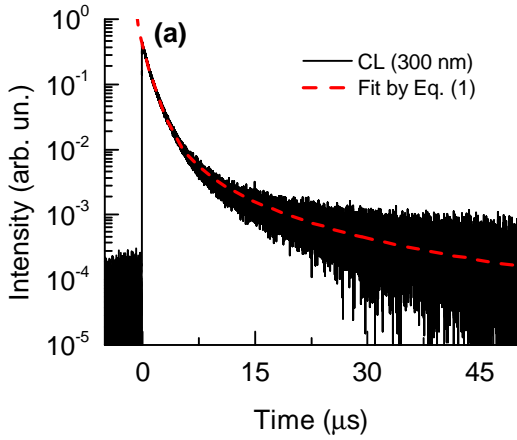


Figure 2: Solid curves – CL kinetics from $(\text{Y}_2\text{Sc}_1)_{0.3}(\text{Sc})[\text{Si}]\text{O}_5$ crystal at 300 (a), 340 (b) and 440 (c). Dashed curves – fitting of these curves by Eq. (1).

the normalizing of the $I_{CL}(t)$ curves on their values at $t = 0$. Due to this normalization, it is possible to analyze the inputs of exponential and hyperbolic decays into the $I_{CL}(t)$ dependence at different wavelengths. It is seen from Table 1, that the relation between the exponential and hyperbolic decays is nearly constant at all wavelengths. However, τ_1 and τ_2 have a significant spectral dependence. Indeed, the $\tau_1(\lambda)$ dependence (λ is a wavelength) is a bell-shaped. The minimal value $\tau_1 \sim 1050$ ns is observed at ~ 300 and 440 nm

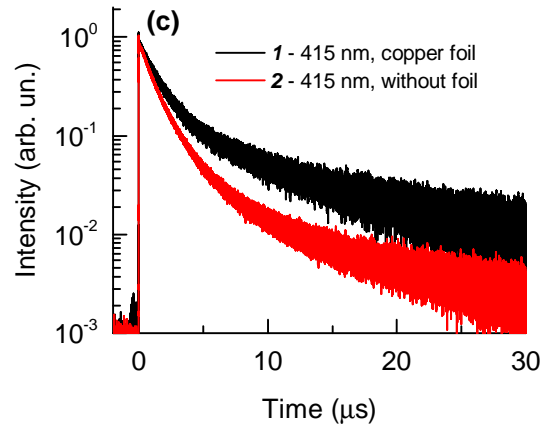
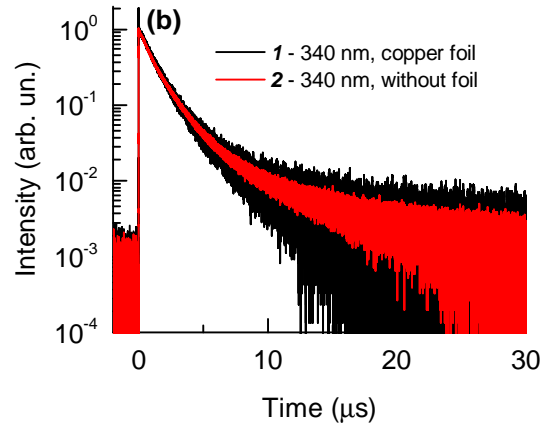
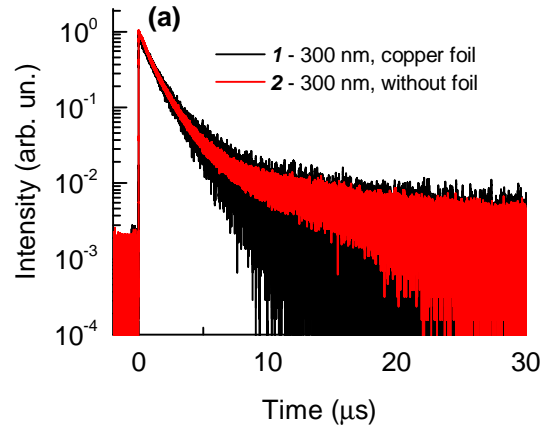


Figure 3: Comparison of CL kinetics from $(\text{Y}_2\text{Sc}_1)_{0.3}(\text{Sc})[\text{Si}]\text{O}_5$ crystal excited by an electron beam after passed through a copper foil with the thickness of $40 \mu\text{m}$ (1) and without passing through any filter (2).

whereas the maximal value $\tau_1 = 1157.2 \pm 0.7$ ns is observed at 370 nm. Simultaneously, τ_2 increases monotonically from 1490 ± 20 ns at 260 nm to 3075 ± 11 ns at 450 nm.

As it is shown in Sec. 3.1, the spectrum CL from a $(\text{Y}_2\text{Sc}_1)_{0.3}(\text{Sc})[\text{Si}]\text{O}_5$ crystal depends on the flux of incident electron beam. In order to find out if the CL kinetics likewise depends on the beam flux, the $I_{CL}(t)$ curves at 300, 340 and 415 nm measured with an electron beam without

passage through a copper foil are compared with the same curves measured when the electron beam passed through the 40 μm copper foil. This comparison is presented in Fig. 3. It is seen from Fig. 3 that at 300 and 340 nm CL kinetics are the same within the experimental error. However, the CL kinetics at 415 nm is significantly different in these cases. Indeed, a bombardment by an electron flow with smaller density occurring in the case of the passage of the beam through the copper foil leads to longer CL decay time in comparison to the initial beam generated by the accelerator.

Thereby, the nonlinear characteristics corresponding to changes in the CL kinetics of $(\text{Y}_2\text{Sc}_1)_{0.3}(\text{Sc})[\text{Si}]\text{O}_5$ crystal are observed only in the visible CL band. These properties in the ultraviolet CL are not found. The difference in dependencies of the CL kinetic parameters on n for different luminescence bands shows that these bands are emitted via different mechanisms. In particular, these bands correspond to different scintillation nonlinearity mechanisms.

3.3. RL amplitude spectrum and kinetics of

$\text{Sc}_{1.318}\text{Y}_{0.655}\text{Si}_{1.013}\text{O}_{4.987}$ crystal

Nonlinear scintillation properties in luminescence from $(\text{Y}_2\text{Sc}_1)_{0.3}(\text{Sc})[\text{Si}]\text{O}_5$ crystal are observed in its RL as well as in its CL. The amplitude spectrum of scintillation from the studied crystal excited by γ -quanta with the energy of 661.7 keV is presented in Fig. 4. The horizontal axis in this figure shows RL energies E_{RL} of each RL pulse in the relative units excited by a single γ -quantum. The vertical axis shows the number of RL pulses having the given E_{RL} . In Fig. 4, at the RL energy $E_{RL} = 1$ rel. un., a photopeak is positioned corresponding to the internal photoelectric effect in Y atoms. During this process, a total absorption of γ -quantum occurs. The photoelectric effect cross-section is proportional to Z^5 where Z is the atomic number [55]. Consequently, the photoelectric effect probability in Y atoms ($Z = 39$) is an order of magnitude higher than that in Sc atoms ($Z = 21$) and is several orders of magnitude higher than the photoelectric effect probability in Si ($Z = 14$) and O ($Z = 8$). Therefore, a photoelectric effect in these atoms can be neglected. Consequently, the photopeak is induced by the electrons ionized from the Y^{3+} K-layer with the binding energy of 17.038 keV [56]. As a result of this photoelectric effect, an electron with the energy of 644.7 keV appears which excites the RL corresponding to the photopeak.

In Fig. 4, at $E_{RL} = 0.65$ rel. un. there is another noticeable peak corresponding to the Compton scattering edge. The energy of Compton electrons corresponding to this edge is of 477 keV and this energy is maximal for Compton electrons induced by γ -quanta with the energies of 661.7 keV [55]. A content of the hard element Y in the crystal is fairly small (~ 8 at. %). Thereby, the Compton effect probability is an order of magnitude higher than the photoelectric effect probability. This fact is illustrated by the numbers of counts corresponding to the photopeak and to the Compton edge (Fig. 4).

Comparison of the photopeak positions in the amplitude spectrum excited by 661.7 keV γ -quanta corresponding to

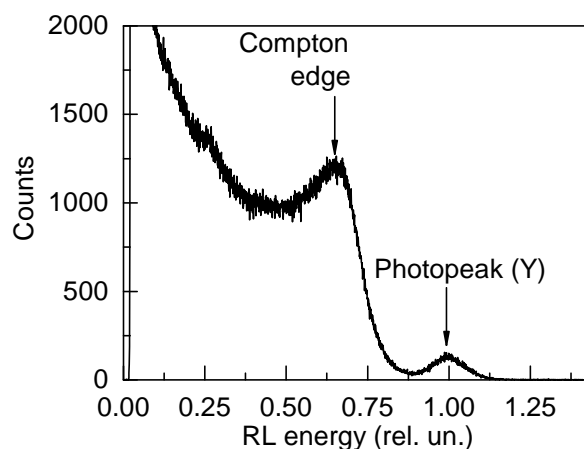


Figure 4: Amplitude spectrum of scintillation from $(\text{Y}_2\text{Sc}_1)_{0.3}(\text{Sc})[\text{Si}]\text{O}_5$ crystal excited by the monochromatic γ -quanta with the energies of 661.7 keV.

$(\text{Y}_2\text{Sc}_1)_{0.3}(\text{Sc})[\text{Si}]\text{O}_5$ crystal and to CeF_3 crystal (for this material, $LY = 2400$ photons/MeV [57]) shown that the LY of $(\text{Y}_2\text{Sc}_1)_{0.3}(\text{Sc})[\text{Si}]\text{O}_5$ intrinsic RL is of 12000 photons/MeV. This value is fairly high and, consequently, this compound in principle can be used as a scintillation material. The photopeak shape of $(\text{Y}_2\text{Sc}_1)_{0.3}(\text{Sc})[\text{Si}]\text{O}_5$ is close to the Gauss curve with the amplitude resolution of 12%. A fairly high LY of intrinsic luminescence generates an advantage of this crystal over analogues based on the activator RL due to its problems with the activator distribution non-homogeneity in grown crystals.

We found that the RL decay times excited by a photoelectron with the energy of 644.7 keV and by a Compton electron with the energy of ≈ 477 keV are different. In order to study the RL kinetics, the RL signal detected by a Hamamatsu R4125Q PMT was measured directly by a Tektronix MSO6-2500BW oscilloscope with the bandwidth of 2.5 GHz. In these measurements, an each $I_{RL}(t)$ curve corresponding to an each single γ -quantum was recorded separately. The duration of each oscillogram was of 100 μs . A total temporal resolution in this experiment was of 3 ns. RL was excited in the same conditions as the spectrum in Fig. 4. We measured $\sim 10^4$ separate $I_{RL}(t)$ curves. An amplitude spectrum calculated using this statistics, is completely similar to that shown in Fig. 4.

The obtained statistics was processed by the following way. A selection of $I_{RL}(t)$ curves corresponding to the photopeak and the Compton edge was made based on the E_{RL} value of each $I_{RL}(t)$ curve. Thereby, the photopeak events fulfilled the $0.9 \text{ rel. un.} \leq E_{RL} \leq 1.1 \text{ rel. un.}$ condition while the Compton edge events fulfilled the $0.65 \text{ rel. un.} \leq E_{RL} \leq 0.9 \text{ rel. un.}$ condition. It is seen that for an analysis of the decay kinetics of RL excited by Compton electrons, we taken into account the events from $E_{RL} = 0.65 \text{ rel. un.}$ (maximum in the amplitude spectrum) to $E_{RL} = 0.9 \text{ rel. un.}$ where the effect of photopeak is still weak. The events with $E_{RL} < 0.65 \text{ rel. un.}$ were not taken into account. Thereby, we studied the RL excited mainly by electrons with the energies

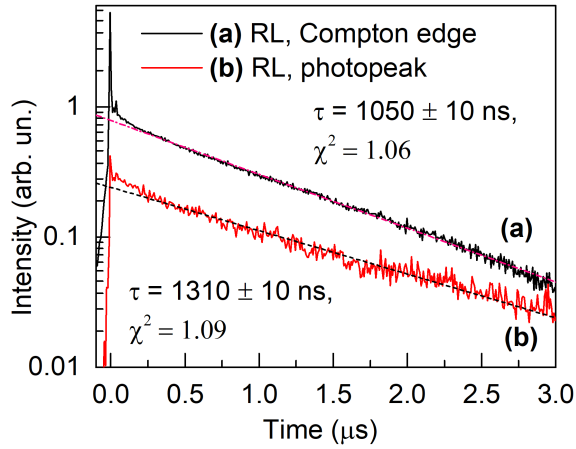


Figure 5: The kinetics of RL from $(\text{Y}_2\text{Sc}_1)_{0.3}(\text{Sc})[\text{Si}]\text{O}_5$ crystal excited by (a) Compton electrons with the energies ≈ 477 keV and (b) photoelectrons with the energies of 644.7 keV. Dash and dash-dot lines show the fits of these curves by Eq. (2).

near the Compton scattering edge (477 keV). Averages of these two groups of $I_{RL}(t)$ curves gives the result presented in Fig. 5. The fit of these averaged curves by an equation

$$I(t) = a \exp(-t/\tau) + b, \quad (2)$$

where a , b and τ are the fitting parameters in the time range of 0.2–3 μs shows that the RL excited by a Compton electron with the energy of ≈ 477 keV has the decay time of $\tau = 1050 \pm 10$ ns. Simultaneously, the RL excited by a photoelectron with the energy of 644.7 keV has the decay time of 1310 ± 10 ns. It is seen that an increase in the initial energy of an exciting electron leads to the increase in the RL decay time.

3.4. CL nonlinearity of $\text{Sc}_{1.318}\text{Y}_{0.655}\text{Si}_{1.013}\text{O}_{4.987}$ crystal

According to [1, 2, 3, 4, 5, 6, 7], the main origin of scintillation nonproportionality and other nonlinear scintillation phenomena is on the one hand a nonlinear dependence of the electron range in a medium on the initial electron energy determining the average n in a track and on the other hand a $LY(n)$ dependence governed by the EEs nonlinear quenching. A dependence of the average electron range R in a medium on the initial electron energy E_0 according to Ref. [58] can be simply given by an expression $R(E_0) \propto E_0^{1.265-0.0954 \ln E_0}$ ($E_0 < 1$ MeV, here the units of E_0 are MeVs). A track can be simply described as a cylinder [3, 8], its length can be estimated as R . A track radius r weakly depends on E_0 because it is determined by a free path lengths of slow secondary electrons. Their energies are of ~ 100 eV and weakly depend on E_0 [5]. For a rough estimation, we can neglect this dependence as it was made in Ref. [3]. Thereby, let us assume that the track radius is not changed with the coordinate along a track. Consequently, a volume-average EE density n can be estimated by an order of magnitude as

$$\bar{n} \approx \frac{E_0}{\beta E_g R(E_0) \pi r^2}, \quad (3)$$

where E_g is the bandgap width of a material, βE_g determines the threshold energy of electron–hole pair creation ($\beta \approx 2 \div 3$ is a property of a given medium). Substitution into this formula a $R(E_0)$ dependence published in Refs. [58, 59] gives a following rough estimation of \bar{n} :

$$\bar{n} \approx \frac{(Z_x/M_x)}{0.412 \beta E_g \pi r^2 \rho_x (Z_{Al}/A_{Al})} E_0^{-0.265+0.0954 \ln E_0}. \quad (4)$$

Here ρ_x is the mass density of this medium in g/cm^2 , Z_{Al} and M_{Al} are the aluminum atomic number and atomic weight, correspondingly, Z_x and M_x are the atomic number and atomic weight of studied material. It is seen from Eq. (4) that \bar{n} is a decreasing function of E_0 . Indeed, at $E_0 = 25$ keV \bar{n} is ~ 10 times higher than at $E_0 = 1000$ keV.

An increase in n leads to the increase in a probability of interactions between EEs. Thereby, this process leads to an increase in EEs non-radiative quenching. As a result, it is manifested by a decrease in LY and it can lead to a shortening in the luminescence decay time. In particular, an observed decrease in the RL decay time with the decrease in E_0 can be explained by an increase in nonradiative EEs quenching induced by the increase in n . Analogous dependence of the luminescence decay time on n has the CL at 415 nm.

Simultaneously, we observed that the CL decay times at 300 and 340 nm (Fig. 3a and 3b) are not sensitive to changes in n in our experiment. Thereby, nonlinear scintillation properties of $(\text{Y}_2\text{Sc}_1)_{0.3}(\text{Sc})[\text{Si}]\text{O}_5$ crystal are different at different wavelengths. In order to study this difference, we estimated the $LY(\bar{n})$ at different wavelengths for this material. A method of this estimation is described in detail in [41]. An experimental setup used in this work is similar to described in [41] with a single exception that, in contrast to [41], in this work the samples were not covered with a diaphragm.

We applied the following method of CL nonlinearity estimation. An exciting electron beam in the accelerator is generated due to EEE [48] from a surface of the vacuum diode. During EEE, the total number N of electrons in each single electron shot randomly fluctuates in our case the range from $\sim 10^{10}$ to $\sim 10^{12}$ particles [45, 46]. Therefore, the exciting beam energy is varied by ~ 2 orders. This leads to similar variations in \bar{n} produced by the beam. Previously we shown [41, 42] that in our experiment E_{REF} is proportional to the beam energy E_b . Also, it is shown there that the dependencies of luminescence parameters on n can be obtained by an accumulation of statics for different E_b . Firstly, for each electron pulse, (E_b, E_L) pairs are measured. Each of this values are calculated using the following expressions:

$$E_b = \int_0^{\bar{\tau}_b} I_{REF}(t) dt, \quad E_L = \int_0^{\bar{\tau}} I_{CL}(t) dt. \quad (5)$$

Table 2

 Parameters of $\text{Bi}_4\text{Ge}_3\text{O}_{12}$ and $(\text{Y}_2\text{Sc}_1)_{0,(3)}(\text{Sc})[\text{Si}]\text{O}_5$ crystals

Crystal	Z	M , Da	ρ , g/cm ³	I , eV	E_g , eV	β
$\text{Bi}_4\text{Ge}_3\text{O}_{12}$	529	1246	7.13	182 ¹	4.2 [61, 62]	2.38 [62]
$(\text{Y}_2\text{Sc}_1)_{0,(3)}(\text{Sc})[\text{Si}]\text{O}_5$	107.67	226.59	3.859	138 ²	7.5 ³ [63]	2 [51] ⁴

We based on the relations $E_b \propto E_{REF}$ and $E_L \propto E_{CL}$. The CL yield is given by an expression $LY_{CL} = E_L/E_b$. At each wavelength, 1000 (E_b, E_L) pairs were measured. After that, the obtained data was sorted by E_b in the ascending order. Then the data was divided into groups with 100 pairs in each group. For the each group, average values of (E_b, E_L) and LY and their standard errors were calculated.

An estimation of \bar{n} provided by the exciting electron beam was made by the following method. Here we give only a general scheme of calculations for brevity. In order to obtain detailed information, see Ref. [41]. Regarding the Coulomb repulsion of electrons in the beam, we obtained a common expression for $\bar{n}(E_b)$ dependence with two adjustment parameters determined empirically from experiments [41]. Simultaneously, a $LY(n)$ dependence for $\text{Bi}_4\text{Ge}_3\text{O}_{12}$ crystal was obtained using photoluminescence is published in Ref. [9]. In Ref. [41] we reported that, in our experiment, a EEE electron beam produces in media a EE distribution close to a homogeneous one. Similar distribution is created by a laser radiation. Also, the main origins of nonlinearity (dipole-dipole interaction between and Coulomb interaction between EEs, etc) are related to EEs with the energies near the E_g [1]. Thereby, $LY(n)$ curve measured by the photoluminescence experiment and $LY_{CL}(\bar{n})$ curve should be close to each other. Equating of $LY(n)$ for $\text{Bi}_4\text{Ge}_3\text{O}_{12}$ published in [9] to the $LY_{CL}(\bar{n})$ curve for the same crystal measured in our work leads to determination of two empirical parameters in the $\bar{n}(E_b)$ dependence and therefore each E_b value is linked to corresponding \bar{n} value for $\text{Bi}_4\text{Ge}_3\text{O}_{12}$ crystal. The electron beam exciting CL in $\text{Bi}_4\text{Ge}_3\text{O}_{12}$ and in $(\text{Y}_2\text{Sc}_1)_{0,(3)}(\text{Sc})[\text{Si}]\text{O}_5$ has the same parameters. Thereby, in order to obtain \bar{n} for the studied crystal ($\bar{n}_{Y_{SSO}}$), this value can be recalculated from \bar{n} value for $\text{Bi}_4\text{Ge}_3\text{O}_{12}$ (\bar{n}_{BGO}) using the following equation [41]:

$$\bar{n}_{Y_{SSO}} = \bar{n}_{BGO} \frac{\beta_{BGO} E_g^{BGO} \rho_e^{BGO} \ln \left(1.16 \frac{\langle E_0 \rangle + 2.9 I_{BGO}}{I_{BGO}} \right)}{\beta_{Y_{SSO}} E_g^{Y_{SSO}} \rho_e^{Y_{SSO}} \ln \left(1.16 \frac{\langle E_0 \rangle + 2.9 I_{Y_{SSO}}}{I_{Y_{SSO}}} \right)} \quad (6)$$

In this expression, $\rho_e = \rho Z/M$ is the volume density of the electron number in medium, ρ is its mass density, Z is the atomic number and M is the atomic weight. Also, in Eq. (6), I is the average ionization potential determined by the ESTAR system [60], $\langle E_0 \rangle = 120$ keV is the average energy of electrons in the exciting beam. The values of parameters in Eq. (6) used for calculation are presented in Table 2. Currently, values of E_g and β for $(\text{Y}_2\text{Sc}_1)_{0,(3)}(\text{Sc})[\text{Si}]\text{O}_5$ crystal are unknown. Therefore, we use in our estimations

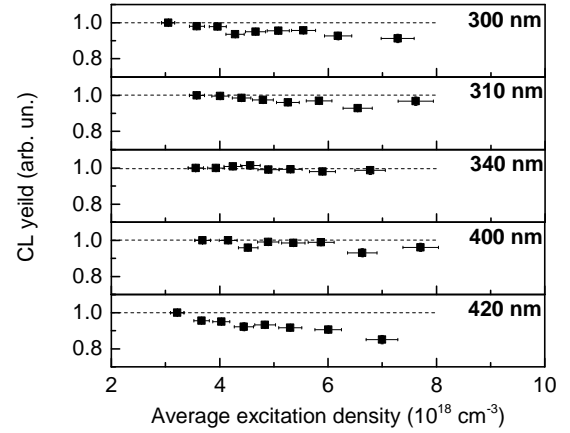


Figure 6: Estimations of CL yield dependence on the volume-averaged EE density for $(\text{Y}_2\text{Sc}_1)_{0,(3)}(\text{Sc})[\text{Si}]\text{O}_5$ crystal at different wavelengths.

these parameters for close materials - Sc_2SiO_5 and Lu_2SiO_5 . According to Ref. [51], $\beta E_g = 15$ eV for Sc_2SiO_5 . Simultaneously, for Lu_2SiO_5 $E_g = 7.5$ eV [63]. Thereby, if we accept that for $(\text{Y}_2\text{Sc}_1)_{0,(3)}(\text{Sc})[\text{Si}]\text{O}_5$ $E_g = 7.5$ eV and $\beta E_g = 15$ eV, an electron-hole threshold is $\beta = 2$. Also, we should recalculate E_b from its value for $\text{Bi}_4\text{Ge}_3\text{O}_{12}$ to the value for $(\text{Y}_2\text{Sc}_1)_{0,(3)}(\text{Sc})[\text{Si}]\text{O}_5$. Indeed, the cross-section of the bremsstrahlung radiation is proportional to ρZ^2 for a given material [55]. Consequently, $E_b^{Y_{SSO}} = \rho_{Y_{SSO}} Z_{Y_{SSO}}^2 E_b^{BGO} / \rho_{BGO} Z_{BGO}^2$.

The results of analysis described above are presented in Fig. 6. It should be noted that \bar{n} values presented in Fig. 6 are the estimates and they are not the accurate values. Errors in Fig. 6 present statistical deviation but they do not take into account any systematic error which is now unknown. Therefore, \bar{n} values in Fig. 6 are the rough estimates in order of magnitude. All curves are normalized on the LY_{CL} values at minimal \bar{n} . Simultaneously, all $LY_{CL}(\bar{n})$ curves in Fig. 6 were measured in similar conditions. Positions of optical fiber, x-ray sensor and crystal were not changed. Therefore, the errors of the relations between the curves are accurately described by the statistical errors presented in Fig. 6.

It is seen from Fig. 6, that obtained $LY_{CL}(\bar{n})$ curves are different at different wavelengths. In general, this situation occurs if luminescence mechanisms of different emission bands are different. For example, this case is observed for CeF_3 [41]. It is concluded from Fig. 6, that in the range of EE densities $(2.5 \div 8) \cdot 10^{18} \text{ cm}^{-3}$ at 340 nm LY_{CL} is nearly constant. However, at 300 and 420 nm LY_{CL} falls with increasing \bar{n} . Indeed, at 300 nm LY_{CL} falls by $\sim 10\%$ and at 420

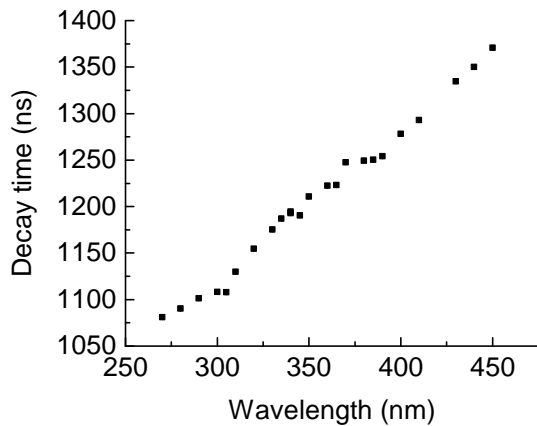


Figure 7: The dependence of the CL decay time on the wavelength for CL from a $(\text{Y}_2\text{Sc}_1)_{0.3}(\text{Sc})[\text{Si}]\text{O}_5$ crystal. Values are obtained by fitting measured $I_{CL}(t)$ dependencies by Eq. (2) in the time range $0 \div 3 \mu\text{s}$ of the curves measured without copper foil.

nm it falls by $\sim 20\%$. Intermediate situations are observed at 310 and 400 nm. The fact that $LY_{CL}(\bar{n})$ dependencies are different at different wavelengths is established.

3.5. Discussion

Let us compare the CL and RL kinetics of scintillation from $(\text{Y}_2\text{Sc}_1)_{0.3}(\text{Sc})[\text{Si}]\text{O}_5$ crystal. For a correct comparison, a fitting of $I_{CL}(t)$ curves by Eq. (2) should be made in similar conditions – in the time range $0-3 \mu\text{s}$. A $\tau_{CL}(\lambda)$ dependence calculated by this method for CL excited by the electron beam without passage through a copper foil is presented in Fig. 7. Unlike the fitting by Eq. (1), this $\tau_{CL}(\lambda)$ dependence is increased monotonically with an increase in λ . In general, it is seen from Fig. 7 that the τ_{CL} values are consistent with the RL decay times (Fig. 5).

Let us calculate τ for CL at 415 nm by the same method for excitation by the initial electron beam and the electron beam passed through the $40 \mu\text{m}$ copper foil (Fig. 3c). Fitting of these dependencies by Eq. (2) in the time range $0-3 \mu\text{s}$ gives $\tau = 1165 \pm 1 \text{ ns}$ for the initial electron beam and $\tau = 1377 \pm 3 \text{ ns}$ in the case of the electron beam with the flux decreased by ~ 20 times. It is seen that these decay times are close to the decay times of RL excited by 477 keV and 644.7 keV electrons. However, τ for CL at 300 and 340 nm are equal for the initial and weakened electron beam within the experimental error.

Therefore, on the one hand, a decrease in \bar{n} leads to the shift of the CL spectrum to shorter wavelengths (Fig. 1). On the other hand, an increase in the energy of single particles associated with the decrease in \bar{n} leads to the increase in τ . However, at shorter wavelengths shorter decay time is observed (Fig. 7). This contradiction is resolved as follows. During the RL measurements, the photosensitivity of the PMT was maximal in visible region. It should be noted that in the visible region the CL band is located whose decay time depends on the energy of exciting electrons. It means

that, during the RL registration, the measured emission is mainly the luminescence from this visible band. On the other hand, the ultraviolet bands with weaker dependencies on \bar{n} are less involved in the formation of the measured $I_{RL}(t)$ dependence. Moreover, a shift of the spectrum into the ultraviolet region leads to the further decrease in the input of these ultraviolet bands into the measured curve.

Despite of the fact that both the shift in CL spectrum and the change in the decay time of scintillation are induced in general by interactions between EEs at their high concentrations, we found that the mechanisms of the shift in the CL spectrum and the change in the scintillation decay time are different. Indeed, a shift in the spectrum with the change in \bar{n} qualitatively differs from those which leads to the change in the scintillation decay time because the observed spectral shift is related to all the observed luminescence bands while the changes in the scintillation kinetics are observed only in the visible luminescence band.

Fig. 6 shows that the $LY_{CL}(\bar{n})$ dependencies are different in the region of $(3 \div 8) \times 10^{18} \text{ cm}^{-3}$ at different wavelengths. We suppose that, for $\bar{n} > 8 \times 10^{18} \text{ cm}^{-3}$, the $LY_{CL}(\bar{n})$ at different λ are also different because an increase in \bar{n} leads to the increase in the EEs interaction probability. Differences between $LY_{CL}(\bar{n})$ at different λ are caused mainly by this interaction. Thereby, an increase in \bar{n} should enhance this difference.

Estimations of \bar{n} for different experiments in this work are presented in Table 3. Firstly, we used Eq. (4) to estimate the average EE density in tracks produced by electrons with the initial energies of 120, 477 and 644.7 keV. In all calculations, we used the value of a track radius r for close oxyorthosilicate crystal $\text{Gd}_2\text{SiO}_5:\text{Ce}$ [3]. It should be noted that the n values estimated using Eq. (4) are slightly overestimated because the average electron range is always slightly less than the actual track length due to the turns of tracks. Also, we estimated \bar{n} using Eq. (3) with the range $R(E_0)$ calculated by the NIST ESTAR system [60]. This calculation is slightly more accurate than that made by Eq. (4). However, Eq. (4) is an analytical one and thereby it provides better understanding of physical process. In the case of a $(\text{Y}_2\text{Sc}_1)_{0.3}(\text{Sc})[\text{Si}]\text{O}_5$ crystal, the values of $R(E_0)$ calculated by the NIST ESTAR system are slightly less than that calculated by expressions published in Refs. [58, 59].

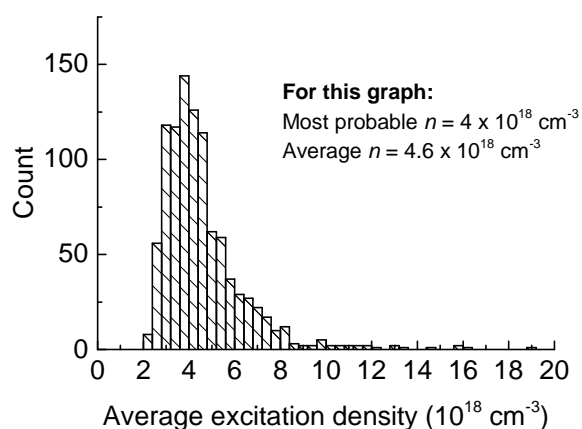
Secondly, we estimated \bar{n} using the method proposed in Ref. [41] (see Sec. 3.4). A high-power electron beam with $N \sim 10^{10}-10^{12}$ produces nearly homogeneous EE distribution due to the significant role of EE diffusion [41]. Indeed, the surface area of the beam is of 2 cm^2 . Thereby, an estimation of the typical distance between the closest tracks δr can be obtained by $\delta r \sim \sqrt{S/N} \approx 10-100 \text{ nm}$. Simultaneously, a typical EE diffusion length during the time of $\sim 1 \text{ ns}$ corresponding to the time of the electron beam existence is of $\sim 100 \text{ nm}$ [5]. Therefore, the tracks strongly overlap.

An example of the EDF of \bar{n} values produced by the electron beam in this work is presented in Fig. 8. The method of \bar{n} determination is described briefly in Sec. 3.4. and in details in Ref. [41]. To obtain this distribution, 991 pulse

Table 3

 Estimations of volume-averaged EE density in $(\text{Y}_2\text{Sc}_1)_{0,(3)}(\text{Sc})[\text{Si}]\text{O}_5$ crystal in RL and CL experiments

Initial energy and type of the exciting electrons	Estimations of \bar{n}
~ 120 keV, dense flow of EEE-electrons, volume distribution of EEs close to uniform one, a significant overlapping between tracks [41]	$3.3 \times 10^{18} \text{ cm}^{-3}$ (by Eq. (4)) $2.5 \times 10^{18} \text{ cm}^{-3}$ (by Eq. (3), R calculated using [60]) $4 \times 10^{18} \text{ cm}^{-3}$ (by the method [41])
~ 120 keV, flow of EEE-electrons after passing the $40 \mu\text{m}$ copper foil, individual tracks with a weak overlapping	$3.3 \times 10^{18} \text{ cm}^{-3}$ (by Eq. (4)) $2.5 \times 10^{18} \text{ cm}^{-3}$ (by Eq. (3), R calculated using [60]) $0.2 \times 10^{18} \text{ cm}^{-3}$ (by the method [41])
477 keV, Compton electron, a single track	$1.6 \times 10^{18} \text{ cm}^{-3}$ (by Eq. (4)) $1.2 \times 10^{18} \text{ cm}^{-3}$ (by Eq. (3), R calculated using [60])
644.7 keV, photoelectron, a single track	$1.4 \times 10^{18} \text{ cm}^{-3}$ (by Eq. (4)) $1.1 \times 10^{18} \text{ cm}^{-3}$ (by Eq. (3), R calculated using [60])


Figure 8: A typical view of EDF for volume-averaged EE densities created by an electron beam in $(\text{Y}_2\text{Sc}_1)_{0,(3)}(\text{Sc})[\text{Si}]\text{O}_5$ crystal without passing through a copper foil.

of accelerator was analyzed. It is seen from Fig. 8 that the minimal value of \bar{n} in this figure is of $2 \times 10^{18} \text{ cm}^{-3}$, the most probable \bar{n} value is of $4 \times 10^{18} \text{ cm}^{-3}$ and the average value is of $4.6 \times 10^{18} \text{ cm}^{-3}$. Simultaneously, for a single track, $\bar{n} = 3.3 \times 10^{18} \text{ cm}^{-3}$ (estimation by Eq. (4)) and $\bar{n} = 2.5 \times 10^{18} \text{ cm}^{-3}$ (estimation by Eq. (3) which R calculated by the NIST ESTAR). Thereby, mainly, in the case of EEs created by the high-power electron beam, \bar{n} is higher than the \bar{n} in a single track. This fact shows that the tracks are significantly overlapped. Therefore, in this case, $\bar{n} \sim 4 \times 10^{18} \text{ cm}^{-3}$.

Excitation of CL by the electron beam after passing through the $40 \mu\text{m}$ copper foil differs from that produced by the initial electron beam. Indeed, in the case of electron beam passed through the foil, N is less by ~ 20 times. Simultaneously, the EEDF is changed very little therefore we assume that the average energy of particles in the beam is not changed ($\langle E_0 \rangle \approx 120$ keV). Consequently, for the excitation by the beam passed through the foil, $\delta r \sim 40\text{--}400$ nm and an overlapping between the tracks still occurs but its role is significantly weaker. The most of tracks in this case are

individual and they do not interact. This fact is proved by the following analysis. Division of the \bar{n} value calculated for the initial electron beam by 20 gives the EE density of $0.2 \times 10^{18} \text{ cm}^{-3}$. This value is an order of magnitude smaller than the \bar{n} for the individual track ($3.3 \times 10^{18} \text{ cm}^{-3}$ according to Eq. (4) and $2.5 \times 10^{18} \text{ cm}^{-3}$ according to Eq. (3) with the range calculated by the NIST ESTAR). Thereby, in this case, the individual non-interacting tracks are formed with the average EE density of $\sim 3 \times 10^{18} \text{ cm}^{-3}$ in each of them. Consequently, a correct EE density estimation for the excited area in this experiment is of $\sim 3 \times 10^{18} \text{ cm}^{-3}$.

Therefore, in the case of CL at 415 nm, a $\sim 30\%$ decrease in \bar{n} leads to the 18% increase in τ from 1165 ± 1 ns to 1377 ± 3 ns. In the case of single γ -quanta, a $\sim 10\%$ decrease in \bar{n} caused by the increase in the exciting electron energy from 477 keV to 644 keV leads to the 25% increase in τ from 1050 ± 10 ns to 1310 ± 10 ns. It is seen that the results obtained from CL and RL are consistent. A difference can be caused on the one hand by the fact that the EEDF in CL is wide and consists of electrons with different energies while the RL is excited by the monochromatic particles and on the other hand the RL was measured integrally over the wavelengths while CL was measured monochromatically.

Let us estimate typical spatial scales of EEs corresponding to the emission in the visible region. An increase in \bar{n} corresponds to the decrease in typical distances between EEs. The studied phenomena are observed at $\bar{n} \sim 10^{18} \text{ cm}^{-3}$. This density corresponds to the typical distances between EEs of ~ 10 nm. Therefore, at this distances, the EEs corresponding for the visible luminescence notably interact with each other while the interaction between the EEs corresponding to the ultraviolet luminescence is much weaker. In general, the mechanisms of $LY_{CL}(\bar{n})$ dependence are also related to EEs interaction. However, our results show that in the case of $(\text{Y}_2\text{Sc}_1)_{0,(3)}(\text{Sc})[\text{Si}]\text{O}_5$ crystal these nonlinear scintillation properties occurs via different mechanisms.

As it was mentioned in Sec. 3.1, the spectral and kinetic properties of the luminescence from $(\text{Y}_2\text{Sc}_1)_{0,(3)}(\text{Sc})[\text{Si}]\text{O}_5$ crystal are in general close to the same characteristics of LuScSiO_5 [50], Sc_2SiO_5 [51, 52] and Sc_2O_3 [53, 54]. A

mechanism of Sc_2O_3 intrinsic luminescence was studied in Ref. [53]. Authors [53] did not find in the reflectance spectrum any excitonic peak. Consequently, a bright intrinsic luminescence from Sc_2O_3 at 340 nm cannot currently be related to STE radiative decay. Authors [53] noted that the characteristics of this luminescence are typical for a tunneling recombination of spatially correlated electrons and holes captured in traps. A similar conclusion was made in Ref. [52] in regard with intrinsic luminescence of Sc_2SiO_5 .

A similarity in the spectral and kinetic parameters of luminescence from $(\text{Y}_2\text{Sc}_1)_{0,(3)}(\text{Sc})[\text{Si}]\text{O}_5$ to the same parameters for LuScSiO_5 , Sc_2SiO_5 and Sc_2O_3 shows that the mechanisms of luminescence from these materials are also similar. The recombination can occur due to transitions in crystalline defects. In particular, in nonactivated orthosilicates, the emission centers can be related to oxygen vacancies [64].

4. Conclusion

$(\text{Y}_2\text{Sc}_1)_{0,(3)}(\text{Sc})[\text{Si}]\text{O}_5$ crystal has a fairly bright intrinsic luminescence at room temperature excited by both electrons with the energies of 50-300 keV and γ -quanta with the energy of 661.7 keV. The light yield of scintillation excited by the γ -quanta is of 12000 photons/MeV. Thereby, this crystal generates interest for practical applications. The Compton effect probability in the crystal is an order of magnitude higher than the photoeffect probability due to the predomination of light elements (Sc, Si and O) in the crystal structure. This leads to formation of a pronounced Compton scattering edge in the amplitude spectrum.

In general, the spectral and kinetic parameters of intrinsic luminescence from $(\text{Y}_2\text{Sc}_1)_{0,(3)}(\text{Sc})[\text{Si}]\text{O}_5$ are close to that for related oxides containing Sc^{3+} . The kinetics of $(\text{Y}_2\text{Sc}_1)_{0,(3)}(\text{Sc})[\text{Si}]\text{O}_5$ consists of two stages. The first stage is a single-exponent one with the decay time of ~ 1.0 - $1.3 \mu\text{s}$. The second stage dominates till $\sim 10 \mu\text{s}$ after the beginning of the emission and corresponds to a hyperbolic Becquerel decay with the power of -2.

The scintillation from $(\text{Y}_2\text{Sc}_1)_{0,(3)}(\text{Sc})[\text{Si}]\text{O}_5$ crystal has nonlinear properties. The decay time of RL excited by a photoelectron with the energy of 644.7 keV is of 1310 ± 10 ns while in the case of a Compton electron with the energy of 477 keV the decay time is of 1050 ± 10 ns. The CL decay time at 415 nm excited by the EEE beam with the average energy of 120 keV is of 1165 ± 1 ns. A decrease in the fluence of the beam by ~ 20 times leads to an increase in the CL decay time to 1377 ± 3 ns. Simultaneously, the decay times at 300 and 340 nm in our experiment do not depend on the average EE density. The CL spectrum of $(\text{Y}_2\text{Sc}_1)_{0,(3)}(\text{Sc})[\text{Si}]\text{O}_5$ crystal also depends on the average EE density. Indeed, a decrease in the flux of the exciting electron beam by ~ 20 times leads to the shift in spectrum from 340 to 315 nm.

The observed nonlinear parameters of intrinsic scintillation from $(\text{Y}_2\text{Sc}_1)_{0,(3)}(\text{Sc})[\text{Si}]\text{O}_5$ are subdivided into

two independent types. A change in the temporal scintillation parameters induced by the change in the average EE density belongs to properties of the first type. These properties are found only in the visible luminescence from $(\text{Y}_2\text{Sc}_1)_{0,(3)}(\text{Sc})[\text{Si}]\text{O}_5$ crystal. We did not find these properties in its ultraviolet luminescence.

A shift in the CL spectrum induced by the change in the average EE density belongs to properties of the second type. This effect is explained by the differences in the $LY(\bar{n})$ dependencies at different wavelengths corresponding to different emission bands including those located in the ultraviolet region. Different dependencies of LY on \bar{n} lead to the different energy spectral density distributions formed at different \bar{n} .

A decrease in the decay time of scintillation from $(\text{Y}_2\text{Sc}_1)_{0,(3)}(\text{Sc})[\text{Si}]\text{O}_5$ crystal in the visible region accompanied by a decrease in the average EE density is explained by an increase in the nonradiative EEs quenching due to their interaction. This quenching occurs at the distances between EEs of ~ 10 nm.

5. Acknowledgment

The work is supported by Russian Science Foundation (project # 19-79-30086).

References

- [1] A. N. Vasil'ev, From luminescence non-linearity to scintillation non-proportionality, IEEE Transactions on Nuclear Science 55 (2008) 1054–1061. doi:10.1109/TNS.2007.914367.
- [2] J. E. Jaffe, Energy and length scales in scintillator nonproportionality, Nuclear Instruments and Methods in Physics Research Section A: Accelerators, Spectrometers, Detectors and Associated Equipment. 105 (2009) 1378–1382. doi:https://doi.org/10.1016/j.nima.2007.07.059.
- [3] G. Bizarri, W. W. Moses, J. Singh, A. N. Vasil'ev, R. T. Williams, An analytical model of nonproportional scintillator light yield in terms of recombination rates, Journal of Applied Physics 105 (2009) 044507. doi:https://doi.org/10.1063/1.3081651.
- [4] S. A. Payne, W. W. Moses, S. Sheets, L. Ahle, N. J. Cherepy, N. J. Sturm, S. Dazeley, G. Bizarri, W.-S. Choong, Nonproportionality of scintillator detectors: Theory and experiment, IEEE Transactions on Nuclear Science 56 (2009) 2506–2512. doi:10.1109/TNS.2009.2023657.
- [5] G. Bizarri, W. W. Moses, J. Singh, A. N. Vasil'ev, R. T. Williams, The role of different linear and non-linear channels of relaxation in scintillator non-proportionality, Journal of Luminescence 129 (2009) 1790–1793. doi:https://doi.org/10.1016/j.jlumin.2008.12.024.

- [6] Q. Li, J. Q. Grim, R. T. Williams, G. A. Bizarri, W. W. Moses, A transport-based model of material trends in nonproportionality of scintillators, *Journal of Applied Physics* 109 (2011) 123716. doi:<https://doi.org/10.1063/1.3600070>.
- [7] S. A. Payne, M. W. W., S. Sheets, L. Ahle, N. J. Cherepy, B. Sturm, S. Dazeley, G. Bizarri, W.-S. Choong, Nonproportionality of scintillator detectors: Theory and experiment. ii., *IEEE Transactions on Nuclear Science* 58 (2011) 3392–3402. doi:[10.1109/TNS.2011.2167687](https://doi.org/10.1109/TNS.2011.2167687).
- [8] W. W. Moses, G. A. Bizarri, R. T. Williams, S. A. Payne, A. N. Vasil'ev, J. Singh, Q. Li, J. Q. Grim, W.-S. Choong, The origins of scintillator nonproportionality, *IEEE Transactions on Nuclear Science* 59 (2012) 2038–2044. doi:[10.1109/TNS.2012.2186463](https://doi.org/10.1109/TNS.2012.2186463).
- [9] J. Q. Grim, K. B. Ucer, A. Burger, P. Bhattacharya, E. Tupitsyn, E. Rowe, V. M. Buliga, L. Trefilova, A. Gektin, G. A. Bizarri, W. W. Moses, R. T. Williams, Nonlinear quenching of densely excited states in wide-gap solids, *Physical Review B* 87 (2013) 125117. doi:<https://doi.org/10.1103/PhysRevB.87.125117>.
- [10] P. R. Beck, S. A. Payne, S. Hunter, L. Ahle, N. J. Cherepy, E. L. Swanberg, Nonproportionality of scintillator detectors. v. comparing the gamma and electron response, *IEEE Transactions on Nuclear Science* 62 (2015) 1429–1436. doi:[10.1109/TNS.2015.2414357](https://doi.org/10.1109/TNS.2015.2414357).
- [11] W. Wolszczak, P. Dorenbos, Nonproportional response of scintillators to alpha particle excitation, *IEEE Transactions on Nuclear Science* 64 (2017) 1580–1591. doi:[10.1109/TNS.2017.2699327](https://doi.org/10.1109/TNS.2017.2699327).
- [12] V. A. Pustovarov, A. L. Krymov, E. I. Zinin, Time-resolved luminescence of scintillation crystals under excitation by high intensity synchrotron radiation, *Nuclear Instruments and Methods in Physics Research Section A: Accelerators, Spectrometers, Detectors and Associated Equipment* 359 (1995) 336–338. doi:[https://doi.org/10.1016/0168-9002\(94\)01380-2](https://doi.org/10.1016/0168-9002(94)01380-2).
- [13] M. Kirm, A. Andrejczuk, J. Krzywinski, R. Sobierajski, Influence of excitation density on luminescence decay in y3al5o12:ce and baf2 crystals excited by free electron laser radiation in vuv, *physica status solidi (c)* 2 (2005) 649–652. doi:<https://doi.org/10.1002/pssc.200460255>.
- [14] A. Belsky, B. Carré, N. Fedorov, E. Feldbach, J. Gaudin, S. Guizard, G. Geoffroy, M. De Grazia, M. Kirm, P. Martin, H. Merdji, V. Nagirnyi, G. Petite, Interaction d'impulsions vuv intenses avec les solides luminescents, *J. Phys. IV France* 138 (2006) 155–161. doi:<https://doi.org/10.1051/jp4:2006138018>.
- [15] M. Kirm, V. Babin, E. Feldbach, S. Guizard, M. De Grazia, V. Nagirnyi, A. Vasil'ev, S. Vielhauer, Behaviour of scintillators under xuv free electron laser radiation, *Journal of luminescence* 128 (2008) 732–734. doi:<https://doi.org/10.1016/j.jlumin.2007.10.025>.
- [16] A. Syntfeld-Kazuch, M. Moszynski, L. Swiderski, W. Klamra, N. Antoni, Light pulse shape dependence on γ -ray energy in csi (tl) , *IEEE Transactions on Nuclear Science* 55 (2008) 1246–1250. doi:[10.1109/TNS.2008.922805](https://doi.org/10.1109/TNS.2008.922805).
- [17] V. Nagirnyi, S. Dolgov, R. Grigonis, M. Kirm, L. L. Nagornaya, F. Savikhin, V. Sirutkaitis, S. Vielhauer, V. A., Exciton–exciton interaction in cdwo4 under resonant excitation by intense femtosecond laser pulses, *Nuclear Instruments and Methods in Physics Research Section A: Accelerators, Spectrometers, Detectors and Associated Equipment* 57 (2010) 1182–1186. doi:[10.1109/TNS.2009.2036430](https://doi.org/10.1109/TNS.2009.2036430).
- [18] M. Kirm, V. Nagirnyi, E. Feldbach, M. De Grazia, B. Carré, H. Merdji, S. Guizard, G. Geoffroy, J. Gaudin, N. Fedorov, P. Martin, A. Vasil'ev, A. Belsky, Exciton–exciton interactions in cdwo4 irradiated by intense femtosecond vacuum ultraviolet pulses, *Physical Review B* 79 (2009) 233103. doi:<https://doi.org/10.1103/PhysRevB.79.233103>.
- [19] J. Q. Grim, Q. Li, K. B. Ucer, R. T. Williams, W. W. Moses, Experiments on high excitation density, quenching, and radiative kinetics in csi:tl scintillator, *Nuclear Instruments and Methods in Physics Research Section A: Accelerators, Spectrometers, Detectors and Associated Equipment* 652 (2011) 284–287. doi:<https://doi.org/10.1016/j.nima.2010.07.075>.
- [20] X. Lu, S. Gridin, R. T. Williams, M. R. Mayhugh, A. Gektin, A. Syntfeld-Kazuch, L. Swiderski, M. Moszynski, Energy-dependent scintillation pulse shape and proportionality of decay components for csi:tl : Modeling with transport and rate equations, *Physical Review Applied* 7 (2017) 014007. doi:<https://doi.org/10.1103/PhysRevApplied.7.014007>.
- [21] J. Cang, X. Fang, Z. Zeng, M. Zeng, Y. Liu, Z. Sun, Z. Chen, Ionization-density-dependent scintillation pulse shape and mechanism of luminescence quenching in labr3:ce , *Physical Review Applied* 14 (2020) 064075. doi:<https://doi.org/10.1103/PhysRevApplied.14.064075>.
- [22] K. Wei, D.-W. Hei, J. Liu, Q. Xu, X.-F. Weng, X.-J. Tan, Theoretical analysis and experimental verification of scintillator luminescence nonlinearity based on carrier quenching model, *Acta Physica Sinica* 70 (2021) 242901. doi:[10.7498/aps.70.20210820](https://doi.org/10.7498/aps.70.20210820).
- [23] A. Gektin, A. N. Vasil'ev, V. Suzdal, A. Sobolev, Energy resolution of scintillators in connection with track structure, *IEEE Transactions on Nuclear Science* 67 (2020) 880–887. doi:[10.1109/TNS.2020.2978236](https://doi.org/10.1109/TNS.2020.2978236).

- [24] C. L. Melcher, J. S. Schweitzer, Cerium-doped lutetium oxyorthosilicate: a fast, efficient new scintillator, *IEEE Transactions on Nuclear Science* 39 (1992) 502–505. doi:10.1109/23.159655.
- [25] Y. D. Zavartsev, S. A. Koutovoi, A. I. Zagumennyi, Czochralski growth and characterisation of large $\text{Ce}_3+\text{Lu}_2\text{SiO}_5$ single crystals co-doped with Mg^{2+} or Ca^{2+} or Tb^{3+} for scintillators, *Journal of Crystal Growth* 275 (2005) e2167–e2171. doi:https://doi.org/10.1016/j.jcrysgro.2004.11.290.
- [26] Y. D. Zavartsev, M. V. Zavertyaev, A. I. Zagumennyi, A. F. Zerrouk, V. A. Kozlov, S. A. Koutovoi, New radiation resistant scintillator Lfs-3 for electromagnetic calorimeters, *Bull. Lebedev Phys. Inst.* 40 (2013) 34–38. doi:https://doi.org/10.3103/S1068335613020024.
- [27] V. Kalinnikov, E. Velicheva, A. Rozhdestvensky, Measurement of the lyso: Ce and lyso:ce, ca scintillator response for the electromagnetic calorimeter of the comet experiment, *Physics of Particles and Nuclei Letters* 20 (2023) 995–1001. doi:https://doi.org/10.1134/S1547477123050412.
- [28] K. Takagi, T. Fukazawa, Cerium-activated Gd_2SiO_5 single crystal scintillator, *Physics of Particles and Nuclei Letters* 42 (1983) 43–45. doi:https://doi.org/10.1063/1.93760.
- [29] M. V. Belov, Y. D. Zavartsev, M. V. Zavertyaev, A. I. Zagumennyi, V. A. Kozlov, S. A. Koutovoi, N. V. Pestovskii, S. Y. Savinov, Scintillation properties of oxyorthosilicate crystals $\text{Gd}_2\text{SiO}_5:\text{Ce}^{3+}:\text{Ca}^{2+}$, *Bulletin of the Lebedev Physics Institute* 46 (2019) 259–262. doi:https://doi.org/10.3103/S1068335619080050.
- [30] M. V. Belov, Y. D. Zavartsev, M. V. Zavertyaev, A. I. Zagumennyi, V. A. Kozlov, S. A. Koutovoi, N. V. Pestovskii, S. Y. Savinov, P^{5+} ion doped $\text{Gd}_2\text{SiO}_5:\text{Ce}^{3+}$ scintillation crystal, *Bulletin of the Lebedev Physics Institute* 46 (2020) 8461–8466. doi:https://doi.org/10.3103/S1068335620010029.
- [31] B. K. Brickeen, E. Geathers, Laser performance of Yb^{3+} doped oxyorthosilicates lyso and gyso, *Optics Express* 17 (2009) 8461–8466. doi:https://doi.org/10.1364/OE.17.008461.
- [32] C. W. Thiel, T. Böttger, R. L. Cone, Rare-earth-doped materials for applications in quantum information storage and signal processing, *Journal of Luminescence* 131 (2011) 353–361. doi:10.1016/j.jlumin.2010.12.015.
- [33] S. A. Koutovoi, A. A. Kalachev, Y. D. Zavartsev, A. I. Zagumennyi, V. V. Voronov, V. I. Vlasov, V. I. Eremina, V. F. Tarasov, Chemical composition based on oxyorthosilicates containing yttrium and scandium for quantum electronics (in russian), patent rf, num. ru2693875c1 (2019).
- [34] L. D. Iskhakova, A. B. Ilyukhin, S. A. Kutovoi, V. I. Vlasov, Y. D. Zavartsev, V. F. Tarasov, R. M. Eremina, The crystal structure of new quantum memory-storage material $\text{Sc}_{1.368}\text{Y}_{0.632}\text{SiO}_5$, *Acta Crystallographica Section C: Structural Chemistry* 75 (2019) 1202–1207. doi:https://doi.org/10.1107/S2053229619010507.
- [35] V. I. Solomonov, Kinetics of pulsed cathodoluminescence, *Optics and Spectroscopy* 95 (2003) 248–254. doi:https://doi.org/10.1134/1.1604432.
- [36] D. I. Vaisburd, K. E. Evdokimov, Creation of excitations and defects in insulating materials by high-current-density electron beams of nanosecond pulse duration, *phys. stat. sol. (c)* 2 (2005) 216–222. doi:10.1002/pssc.200460149.
- [37] V. I. Solomonov, S. G. Michailov, A. I. Lipchak, V. V. Osipov, V. G. Shpak, S. A. Shunailov, M. I. Yalandin, M. R. Ulmaskulov, Clavi pulsed cathodoluminescence spectroscope, *Laser physics* 16 (2006) 126–129. doi:https://doi.org/10.1134/S1054660X06010117.
- [38] A. Lushchik, C. Lushchik, K. Schwartz, F. Savikhin, E. Shablonin, A. Shugai, E. Vasil'chenko, Creation and clustering of frenkel defects at high density of electronic excitations in wide-gap materials, *Nuclear Instruments and Methods in Physics Research B* 277 (2012) 40–44. doi:10.1016/j.nimb.2011.12.051.
- [39] V. Solomonov, A. Spirina, What is the Pulsed Cathodoluminescence?, *IntechOpen*, 2012. doi:10.5772/33833. URL https://doi.org/10.5772/33833
- [40] I. N. Ogorodnikov, M. S. Kiseleva, V. Y. Vostrov D. O., Yakovlev, Cathodoluminescence kinetics of $\text{Li}_6\text{Gd}_3\text{O}_9$ crystals, *Journal of Luminescence* 158 (2015) 252–259. doi:https://doi.org/10.1016/j.jlumin.2014.10.011.
- [41] M. V. Belov, S. A. Koutovoi, V. A. Kozlov, N. V. Pestovskii, S. Y. Savinov, A. I. Zagumennyi, Y. D. Zavartsev, M. V. Zavertyaev, Measurement of non-linearity in the cathodoluminescence yield for non-doped scintillators, *Journal of Applied Physics* 130 (2021) 233101. doi:https://doi.org/10.1063/5.0062673.
- [42] M. V. Belov, S. A. Koutovoi, V. A. Kozlov, N. V. Pestovskii, S. Y. Savinov, A. I. Zagumennyi, Y. D. Zavartsev, M. V. Zavertyaev, Interaction of electronic excitations in solid body with each other and with particles of an ambient gas induced during excitation of pulsed cathodoluminescence of media. chapter in “fast electric-explosive, electronic and 22electromagnetic processes in pulse electronics and optoelectronics”, ed. by g.a. mesyats, (in russian) (2023).
- [43] V. I. Solomonov, A. V. Spirina, A. S. Makarova, Features of the pulsed cathodoluminescence kinetics of

- neodymium ion in yttrium-aluminum garnet and yttria, *Physics of the Solid State* 64 (2022) 2088–2092. doi:10.21883/PSS.2022.13.52306.24s.
- [44] M. I. Yalandin, V. I. Solomonov, A. V. Spirina, S. A. Shunailov, K. A. Sharypov, A. S. Makarova, A. I. Lipchak, Specific features of pulsed cathodoluminescence under excitation by nanosecond and subnanosecond electron beams, *Doklady Physics* 68 (2023) 50–55. doi:https://doi.org/10.1134/S1028335823020064.
- [45] V. I. Solomonov, V. V. Osipov, A. S. Makarova, A. V. Spirina, V. V. Platonov, V. A. Shitov, Luminescent response to the transformation of zinc selenide in ceramic synthesis, *Journal of Applied Spectroscopy* 91 (2024) 278–285. doi:https://doi.org/10.1007/s10812-024-01718-8.
- [46] V. N. Afanas'ev, V. B. Bychkov, V. D. Lartsev, V. P. Pudov, V. I. Solomonov, S. A. Shunailov, V. V. Generalova, A. A. Gromov, Parameters of the electron beams generated by the radan-220 and radan-ekspert accelerators, *Instrum. Exp. Tech.* 58 (2005) 641–645. doi:https://doi.org/10.1007/s10786-005-0114-y.
- [47] E. H. Baksht, I. D. Kostyrya, E. I. Lipatov, M. I. Lomaev, D. V. Rybka, V. F. Tarasenko, Excess-energy electrons in a nanosecond electron beam from a vacuum diode., *Tech. Phys.* 52 (2007) 489–494. doi:https://doi.org/10.1134/S1063784207040147.
- [48] G. A. Mesyats, *Explosive Electron Emission*, URO-Press, Ekaterinburg, 1998, 1998.
- [49] M. V. Zavertyaev, V. A. Kozlov, N. V. Pestovskii, A. A. Petrov, A. A. Rodionov, S. Y. Savinov, S. N. Tskhai, Y. D. Zavartsev, A. I. Zagumennyi, S. A. Kutovoi, Emission of molecular nitrogen upon electron bombardment of pyrolytic aerogel SiO_2 and aluminum, *JETP Letters* 110 (2019) 654–658. doi:https://doi.org/10.1134/S0021364019220132.
- [50] M. V. Belov, Y. D. Zavartsev, M. V. Zavertyaev, A. I. Zagumennyi, V. A. Kozlov, S. A. Kutovoi, N. V. Pestovskii, S. Y. Savinov, Scintillation properties of new LuScSiO_5 crystals, *Bull. Lebedev Phys. Inst.* 48 (2021) 97–100. doi:https://doi.org/10.3103/S1068335621040035.
- [51] V. Y. Ivanov, V. L. Petrov, V. A. Pustovarov, B. V. Shulgin, V. V. Vorobjov, E. G. Zinevich, E. I. Zinin, Electronic excitations and energy transfer in a_2SiO_5 -ce (a=y, lu, gd) and sc_2SiO_5 single crystals, *Nuclear Instruments and Methods in Physics Research Section A: Accelerators, Spectrometers, Detectors and Associated Equipment* 470 (2001) 358–362. doi:https://doi.org/10.1016/S0168-9002(01)01054-3.
- [52] V. Y. Ivanov, E. S. Shlygin, V. A. Pustovarov, V. V. Mazurenko, B. V. Shul'gin, Intrinsic luminescence of rare-earth oxyorthosilicates, *Phys. Solid State* 50 (2008) 1692–1698. doi:https://doi.org/10.1134/S1063783408090217.
- [53] A. Lushchik, M. Kirm, C. Lushchik, I. Martinson, G. Zimmerer, Luminescence of free and self-trapped excitons in wide-gap oxides, *Journal of Luminescence* 87 (2000) 232–234. doi:https://doi.org/10.1016/S0022-2313(99)00271-9.
- [54] O. M. Bordun, I. M. Bordun, Luminescence centers in sc_2O_3 , *Journal of Applied Spectroscopy* 64 (1997) 789–792. doi:https://doi.org/10.1007/BF02678861.
- [55] A. I. Akhiezer, V. B. Berestetskii, *Quantum Electrodynamics. Authorized English Ed., Rev. and Enl. by the Authors. Translated from the 2d Russian Ed. Interscience monographs and texts in physics and astronomy, v. 11 Interscience Publishers., Lawrence Berkeley National Laboratory, University of California, 1965.*
- [56] A. C. Thompson, D. Vaughan, *X-ray data booklet*, Interscience, 2001.
- [57] A. J. Wojtowicz, M. Balcerzyk, E. Berman, A. Lempicki, Optical spectroscopy and scintillation mechanisms of $\text{CeLa}_1\text{-xf}_3$, *Physical Review B* 49 (1994) 14880. doi:https://doi.org/10.1103/PhysRevB.49.14880.
- [58] L. Katz, A. S. Penfold, Range-energy relations for electrons and the determination of beta-ray end-point energies by absorption, *Review of Modern Physics* 24 (1952) 28. doi:https://doi.org/10.1103/RevModPhys.24.28.
- [59] I. S. Grigoriev, E. Z. Meilikhov, *Physical values. Handbook. (Fizichseskie velichini, spravochnik. In Russian)*, Energoatomizdat, Moscow, Russia, 1991.
- [60] Nist estar system, <https://physics.nist.gov/PhysRefData/Star/Text/ESTAR-u.html>.
- [61] Z. S. Macedo, A. L. Martinez, A. C. Hernandez, Characterization of $\text{Bi}_4\text{Ge}_3\text{O}_{12}$ single crystal by impedance spectroscopy, *Materials Research* 6 (2003) 577–581. doi:https://doi.org/10.1590/S1516-14392003000400026.
- [62] M. Itoh, T. Katagiri, Intrinsic luminescence from self-trapped excitons in $\text{Bi}_4\text{Ge}_3\text{O}_{12}$ and $\text{Bi}_{12}\text{GeO}_{20}$: Decay kinetics and multiplication of electronic excitations, *Journal of the Physical Society of Japan* 7 (2010) 074717. doi:https://doi.org/10.1143/JPSJ.79.074717.
- [63] M. Kitaura, S. Tanaka, M. Itoh, Optical properties and electronic structure of Lu_2SiO_5 crystals doped with cerium ions: Thermally-activated energy transfer from host to activator, *Journal of Luminescence* 158 (2015) 226–230. doi:https://doi.org/10.1016/j.jlumin.2014.10.010.

- [64] M. V. Belov, S. A. Koutovoi, V. A. Kozlov, N. V. Pestovskii, S. Y. Savinov, A. I. Zagumennyi, Y. D. Zavartsev, M. V. Zavertyaev, Luminescence from oxygen vacancies in Lu_2SiO_5 crystal and ceramics at room temperature, *Journal of Luminescence* 263 (2023) 120155. doi:<https://doi.org/10.1016/j.jlumin.2023.120155>.